LIMITR: Leveraging Local Information for Medical Image-Text Representation

Gefen Dawidowicz [1]   Elad Hirsch [1]   Ayellet Tal [1,2]

[1] Technion – Israel Institute of Technology   [2] Cornell Tech

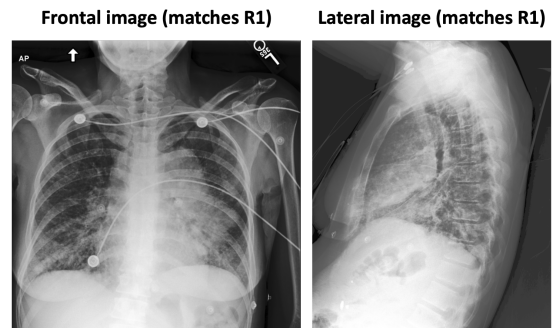{gefen, eladhirsch}@campus.technion.ac.il, ayellet@ee.technion.ac.il

Abstract

Medical imaging analysis plays a critical role in the diagnosis and treatment of various medical conditions. This paper focuses on chest X-ray images and their corresponding radiological reports. It presents a new model that learns a joint X-ray image & report representation. The model is based on a novel alignment scheme between the visual data and the text, which takes into account both local and global information. Furthermore, the model integrates domain-specific information of two types—lateral images and the consistent visual structure of chest images. Our representation is shown to benefit three types of retrieval tasks: text-image retrieval, class-based retrieval, and phrase-grounding. Our code is publicly available [1].

1. Introduction

X-ray imaging is one of the most common medical examinations performed, where in the U.S. alone 70 million scans are performed every year [20]. During a post-scan routine, a medical report is written by a radiologist. This is a challenging task even for trained personnel, since the pathologies, which typically occupy a small portion of the image, might be characterized by subtle (sometimes distributed) anatomical changes. Automating the analysis has the potential to aid experts and to speed-up the process.

The task of producing a joint representation of medical image-report data inherently differs from that of natural image-text, which has been extensively explored recently [6]. The available data is orders of magnitude smaller than that of natural images. Furthermore, the data is highly unbalanced, since most of the examples are normal. Even in abnormal examples, most of the image (/report) is normal.

Due to the importance of the task, the available medical data has been used for a variety of applications, including class-based retrieval (retrieving data of the same diagnosis) [8, 27, 17, 25], pathology classification [23, 8, 3, 27,

R1 PA and lateral views of the chest provided. Large left perihilar opacity is concerning for metastasis. Extensive bilateral pulmonary nodular opacities are concerning for diffuse metastatic lesions, difficult to exclude underlying edema. No large pleural effusion or pneumothorax. Heart size is difficult to assess. The image bony structures appear intact.

R2 The lungs are mildly hyperinflated. The cardiomediastinal silhouette is stable. No CHF, focal infiltrate or effusion is identified. At the right lung apex, there is a tiny (3.1 mm) nodular opacity projecting over right lung apex. No pneumothorax.

Figure 1: **Image-report retrieval.** Given the visual data, which contains both Lung Opacity & Lung Lesion diagnoses, our model retrieves the correct **R1** report. Another report, **R2**, which corresponds to another image, contains the same pathologies. It differs in the subtle details: pathology description, localization, uncertainties, normalities and additional unlabelled pathologies. In tasks such as class-based retrieval, **R2** is considered a correct match. Our model aims also at tasks, such as image-text retrieval, which care about the subtleties.

17, 25], detection [8, 3, 23, 18], and phrase-grounding [3]. Often, these tasks do not require subtle details, such as the severity of the pathology, its exact location, or findings that are beyond the pre-defined pathologies.

We propose a novel model, which learns a joint X-ray image-report representation that is attentive to subtle details, additional descriptions of the pathologies, uncertainties etc., as illustrated in Figure 1. It is based on three key ideas. First, our method learns to utilize both global align-

---

[1] https://github.com/gefend/LIMITR

ment (image-report pairs) that captures high-level information, such as the sheer existence of a disease, and local alignments (region-word pairs) that capture subtle details and abnormalities. Second, it benefits from lateral images, which are usually ignored. Third, it utilizes domain-specific localization information. We elaborate below.

Local alignment in medical imaging is challenging since the data is not annotated locally by bounding boxes and their labels. This is in contrast to natural image datasets, which provide localized ground-truth information [4, 9, 13, 14, 15, 16]. Furthermore, localization ambiguity is inherent in medical imaging, as report findings may correspond to multiple image regions. To this end, we propose a new aggregation method and a new loss, which synthesize both region-word alignments within a single pair and global and local alignments across pairs.

Second, we propose to use lateral views, if they exist, just like radiologists do. These views may provide additional information, yet they are largely ignored by other representation learning works. We introduce an attention model that learns for each portion of the report when to consider both images, when only one, and when none.

Lastly, our model utilizes some basic domain-specific localization information—the structure of the human body; for instance, the heart is always inbetween the lungs and is approximately in the same image position. We show that we can add global positional encoding for the whole dataset. This encoding also allows the network to better learn local connections between the frontal and the lateral views.

To demonstrate the benefit of our model, we evaluate it for three different retrieval tasks: (1) *Text-image retrieval:* Given a report, the goal is to find the most suitable image and vice versa. In this task, we expect the corresponding report (/image) to be retrieved, as illustrated in Figure 1, where all the information that appears in the text and in the image, are taken into account. This task demonstrates the ability of our method to accurately capture subtleties. (2) *Phrase-grounding:* Given an image and a corresponding phrase, the goal is to produce an attention map of the similarity between the phrase and each region. This task demonstrates the quality of the local alignment. (3) *Class-based retrieval:* Given a textual description, the goal is to retrieve images that belong to the same class of the description. This is the most common retrieval task. We present SoTA results for all these tasks.

Hence, our work makes the following contributions:

1. We propose a novel model for learning a joint X-ray image & report representation. It is based on a new local and global alignment scheme. This alignment is shown to boost performance.

2. Our model integrates additional domain-specific knowledge—lateral images and visual structure. This information further improves performance.

3. The benefit of our model is demonstrated on three retrieval tasks, showing its ability to capture fine features in both images and reports. We demonstrate SoTA results on commonly-used datasets.

2. Related work

Recent works on text-image multi-modal representations for *chest X-ray (CXR)* datasets are used for a variety of tasks. These tasks are either uni-modal or multi-modal, as briefly reviewed hereafter.

Uni-modal tasks. The common uni-modal tasks are visual, where the focus is on classification and localization. Specifically, given an image, the goal of [3, 8, 23, 25, 27] is to classify it into pre-defined diagnoses. This can be done for multi-label classes [8, 23, 25, 27] or for binary classification [3, 8, 23, 27].

In localization, we are given images and aim to learn localized information for detection and segmentation tasks [3, 8, 18, 23]. These tasks are designed for single-pathology studies and rely on relatively small datasets. Examples include RSNA pneumonia detection [19], foreign objects detection [26] and SIIM pneumothorax segmentation [1].

Textual analysis in this domain is less prevalent. In [3], the focus is on CXR domain-specific language understanding tasks, such as text classification and masked-token prediction. The joint training with the images provides a superior language model for these tasks.

Multi-modal tasks. Our focus is on multi-modal tasks, for which there exist less works. In [8, 27, 25] the task is *class-based retrieval*, i.e. given an example in one modality (image/text), retrieve examples from the other modality. The requirement is that the retrieved examples should belong to the same class of diagnoses as the query.

In *phrase-grounding*, introduced by [3], we are given an image and a corresponding phrase describing a pathology in the image, and aim to localize the image regions that match the phrase. This is a challenging task as specific relations between phrases and certain image features need to be learned. However, this work ignores studies with multiple pathologies, as well as more elaborated phrases that express uncertainties and descriptions of normalities.

We introduce an additional retrieval task, *text-image (or image-text) retrieval*, where the accuracy of the representation can be better evaluated. We expect to retrieve the exact match from one modality, given the other.

3. Model

Our goal is to learn an informative joint representation of X-ray images and their reports. In this joint representation space, an image and its corresponding report should be mapped to close points, whereas mismatched pairs should reside farther apart. Recall that our model realizes three key
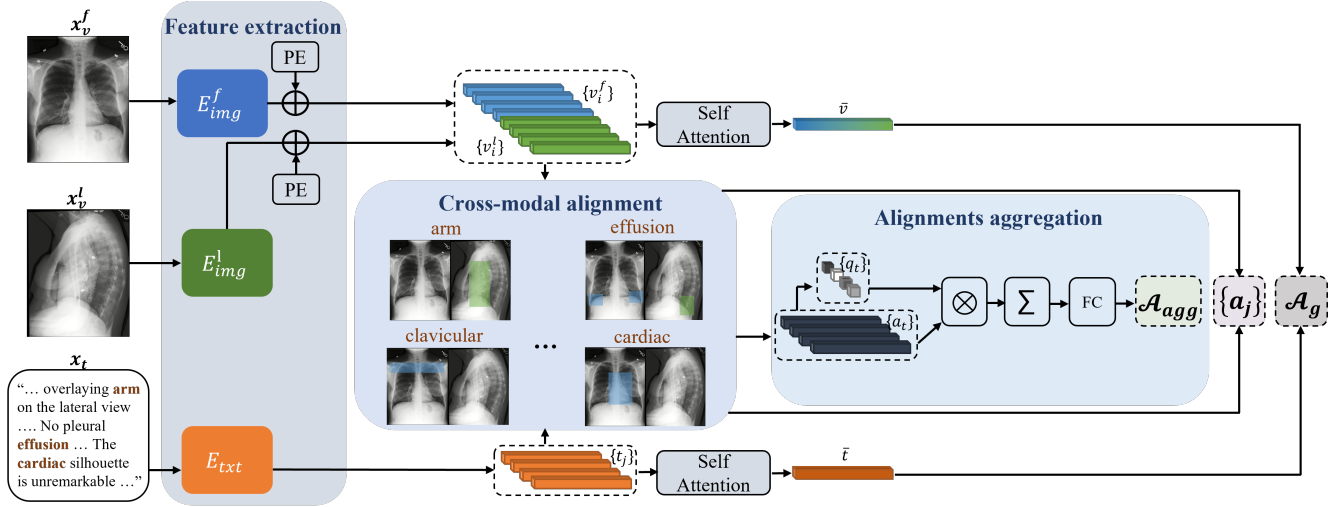
Figure 2: **Model.** The model consists of three blocks. (1) For feature extraction, two CNNs, E_{img}^{l} & E_{img}^{f} for the lateral & the frontal images, are used as the image encoders and one pre-trained network, E_{txt}, is used as the text encoder. The local visual representations are concatenated and a global representation is created using self-attention. A global representation is similarly created for the report. The distance between these representations forms our global alignment $\mathcal{A}_g$, which is used in our global loss, L_g. (2) During cross-modal alignment, alignments between the local representations of the two modalities are calculated (Figure 3). These alignments, $\{a_j\}$, are used for our local internal loss L_{int} (Figure 5). Thanks to our attention mechanism, the model works well with or without lateral images. (3) The local alignments are aggregated using learned significance scores, to create the final image-report similarity score, $\mathcal{A}_{agg}$. These scores are used in our local external loss L_{ext} (Figure 4).

ideas. First, to account for the different importance of the local image regions (/report words) to the global alignment, we propose a novel aggregation method of the local representations, which incorporates learned importance. Second, our model is the first to use lateral images for representation learning, in addition to the frontal ones, when available. Third, our model leverages the fact that medical images are characterized by a unique and known structure of the human body.

Our model, which is outlined in Figure 2, consists of three parts: (1) feature extraction, which produces the local and the global representations, (2) cross-modal alignment, which utilizes these features, as well as additional information, in order to find the alignments between the two modalities, and (3) local-alignment aggregation, which produces global alignment of an image and a report. Our model optimizes the following loss (which will be elaborated upon in Section 3.4):

$$L = L_g + L_{ext} + L_{int}. \qquad (1)$$

Here, the global alignment is optimized by L_g, the local alignment of regions & words across examples is optimized by L_{ext}, and the local alignment of regions & words within a single example is optimized by L_{int}.

3.1. Feature extraction

Given an image x_v and its corresponding report x_t, the visual and the textual features, are independently extracted. Recall that in medical imaging, we lack local annotated data (bounding boxes and their labels); furthermore, the images suffer from localization ambiguity, as findings may correspond to multiple image regions. Thus, pre-trained object detectors are not as useful as in the natural domain.

Visual feature extraction. We benefit from the localized nature of the intermediate layers of CNNs (E_{img} in Fig. 2), to obtain N_r region-level visual features $\{v_1, ..., v_{N_r}\}$. In particular, we use the output of the last *convolution* layer.

Next, we enrich the extracted features with our knowledge of the layout of the human body. Specifically, in chest X-ray the organs are approximately in the same positions (which guide radiologists in the diagnosis process). We leverage this structure by encoding and integrating it within learning. We realize it through adding positional encoding. Since our positional encoding is inherent in the input, it conceptually differs from that being used in *transformers*, which encode the relative positions. We sum each visual local feature vector v_i with a corresponding vector that encodes its spatial $2D$ position. In our implementation we use the $2D$ sinusoidal encoding of [5], as follows. Let v_i be the ith-patch features in the image and $(x, y)_i$ be the coordi-

nates of this patch. Our visual feature vector is then defined as the sum of the visual encoder output with the positional encoding corresponding to the patch location in the image $v_i \leftarrow v_i + PE((x,y)_i)$, where $PE((x,y)_i)$ is that of [5].

We observe that not all local regions are as important. Specifically, some small regions—those that contain abnormalities—should count more than others. To this end, we apply the self-attention operator of [22] on the local features, in order to extract our global image feature representation, $\bar{v}$. This $\bar{v}$ captures the relationships between all the local representations of a given image x_v.

In our implementation we use *Resnet-50* [7] as the image encoder E_{img}, as it has been previously shown to benefit medical images [3, 8, 27].

Frontal and lateral information. Lateral images, which exist in 50% of the studies, contain information that may improve diagnosis, yet they are largely ignored. Our approach utilizes the information from the lateral images, by learning to weigh information from both views. In addition, as studies do not necessarily contain the lateral view, our model learns from studies with a single view, as well as from studies with both views. Specifically, for each view type, we train a separate image encoder, E^l_{img} and E^f_{img}. The features from the two encoders are concatenated to form the set $\left\{ v^f_1, ..., v^f_{N_r}, v^l_1, ..., v^l_{N_r} \right\}$ and are inserted to the cross-modal alignment module. When a lateral image is not available, we set $\left\{ v^l_i \right\}^{N_r}_{i=1} = \mathbf{0}$.

Textual features extraction. Given a report x_t, it is first tokenized, using the vocabulary of [2]. The sequence of tokens is then fed into a text encoder, E_{txt}. This yields local textual features, at the token level, $\{t_1, ..., t_{N_w}\}$. Lastly, since in analogy to image regions, certain words are more important than others, we apply self-attention to extract the global textual features, $\bar{t}$.

In our implementation, we use BioClinicalBERT [2] as our text encoder, due to its high performance.

3.2. Cross-modal alignment

Given a visual and textual local representations, $\{v_1, ..., v_{N_r}\}$ and $\{t_1, ..., t_{N_w}\}$ respectively, our goal is to learn the alignments between the two modalities, including the alignments between report words and image regions. To do that, our model should address two challenges: (1) the lack of local annotations connecting the two modalities, (2) the pathologies may occupy only a small area of the image, as well as a small part of the report. To this end, a fine-grained approach is sought-after.

Our approach, which is illustrated in Figure 3, takes into account the global representations of images and reports, as well as the local representations of regions and words. This is done both by weighing the image region features with respect to each textual feature and vice versa—by weighing the textual features with respect to each region feature. For
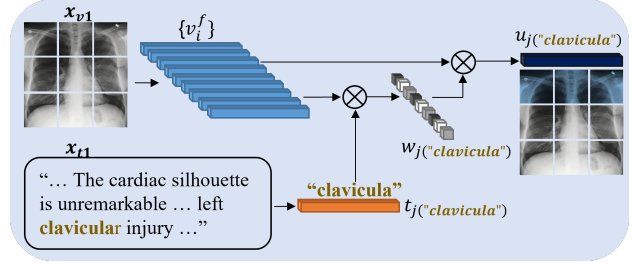

Figure 3: **Cross-modal alignment.** Given an image-report pair (x_v, x_t), we compute for each word t_j (e.g. clavicula) its corresponding visual weighted representation u_j. This is done by using the similarity between each region representation v^f_i to t_j as the weight for this region $w_j[i]$. The right image shows that the regions that correspond to "clavicula" are highlighted in blue, representing the higher weight of these regions. The final visual representation, u_j, is created by a weighted sum of v^f_i.

clarity, in the following we will describe only how this is done in the first case (weighing image regions with respect to text). However, in the loss, both are summed.

First, the cosine similarity c_{ij} between v_i and t_j is computed, to create $c_j = [c_{1j}, c_{2j}, ..., c_{N_rj}]$. It is further normalized using softmax, in order to get an attention weight:

$$w_j = softmax(\lambda c_j). \tag{2}$$

The attended visual feature u_j with respect to the jth word is the weighted sum of all the visual local representations:

$$u_j = \sum_{i=1}^{N_r} w_j[i] \cdot v_i. \tag{3}$$

Next, we calculate the alignment between t_j and its corresponding u_j. The local alignment a_j is calculated as:

$$a_j = \mathcal{A}(u_j, t_j) = \frac{u_j \circ t_j}{\|u_j \circ t_j\|_2}, \tag{4}$$

where $\circ$ is an element-wise multiplication and $\|\cdot\|_2$ is the L_2-norm. Note that unlike [8, 18, 24], our alignment a_j is a vector rather than a scalar (that averages the entries). This is important for our aggregation method, as will be discussed in Section 3.3, where we learn the importance of the different a_j's. Our alignments $\{a_j\}$ will be later used for the local alignment loss L_{int}.

Similarly to the local alignments, we compute the global alignment, given the global image feature vector, $\bar{v}$ and the global report feature vector, $\bar{t}$. It is computed as:

$$\mathcal{A}_g = \mathcal{A}(\bar{v}, \bar{t}) = \frac{\bar{v} \circ \bar{t}}{\|\bar{v} \circ \bar{t}\|_2}. \tag{5}$$

This $\mathcal{A}_g$ will be later used for the global loss L_g.

The cross-modal alignment is computed between each region in both the frontal and the lateral images to each token of the report. Hence, if significant information appears in the two images, regions from both receive high weights. But, when important information appears only in one of the images, only its regions will get high weights. In a sense, our model mimics the radiologists actions. When a pathology is available in the two views, they examine both; otherwise, they focus on the relevant view.

3.3. Aggregation

Our goal is to aggregate all the local alignments of a given image-report pair, in order to create the final representation of the pair, a_f. We do not wish to simply sum the alignments [8], since not all regions should be treated equally. In particular, most image regions and their corresponding report descriptions are normal observations, shared by all examples in the dataset, whereas the pathologies mostly occupy small regions. The distinct information, e.g. the pathology, should be given more weight.

To account for this variance, we suggest to weigh the local alignments in accordance with their informativeness. Let the local alignments, computed at the alignment module, be $\mathcal{A}_T = \{a_1, a_2, a_3...a_{N_w}\}$ (Equation 4). These alignments are aggregated into a single alignment vector using a weighted sum. The weight of each vector is computed by self-attention, where (through the interaction between the local regions) it is determined which should be more attended, in order to better perform the task. Thus, for each a_t we compute its weight relative to the set $\mathcal{A}_T$. Let $\bar{a}$ be the mean of $\mathcal{A}_T$. The weight of a_t is defined as:

$$q_t = \left(softmax\left(\frac{W_q \, \bar{a} \cdot (W_k \, \mathcal{A}_T)^T}{\sqrt{d}} \right) \right)_t, \qquad (6)$$

where $1 \leq t \leq N_w$, W_q and W_k are linear transformations of the self-attention, and d is the feature dimension.

The final alignment vector between an image and a report is defined as:

$$a_f = \sum_{t=1}^{N_w} q_t \, (W_v \cdot a_t). \qquad (7)$$

This aggregated alignment vector represents the image-report pair. It is passed through an FC layer to produce the final scalar alignment score $\mathcal{A}_{agg}$, which will be later used for the external loss L_{ext}.

3.4. Loss

Recall that our goal is to maximize the similarity between positive image-report pairs and minimize the similarity between negative pairs. To achieve this, we use three instances of the contrastive loss function [21], each expressing a different concept: one global and two local, as seen in Equation 1. The latter two enable different regions or words to be considered as having different significance. We elaborate on these losses hereafter.

The global loss, L_g, attempts to maximize the global alignment $\mathcal{A}_g$ (Equation 5) of positive image-report pairs and minimize the global alignment of negative pairs. Let (x_v^k, x_t^k) be a corresponding pair and τ be a temperature parameter. The loss is defined as:

$$L_g(x_v^k, x_t^k) = l^{x_v^k|x_t} + l^{x_t^k|x_v},$$
$$l^{x_v^k|x_t} = -log\left(\frac{exp(\mathcal{A}_g(x_v^k, x_t^k)/\tau)}{\sum_{j=1}^{N} exp(\mathcal{A}_g(x_v^k, x_t^j)/\tau)} \right), \qquad (8)$$
$$l^{x_t^k|x_v} = -log\left(\frac{exp(\mathcal{A}_g(x_v^k, x_t^k)/\tau)}{\sum_{j=1}^{N} exp(\mathcal{A}_g(x_v^j, x_t^k)/\tau)} \right).$$

Here, for a given x_v^k, $l^{x_v^k|x_t}$ aims to increase its similarity to its corresponding report and decrease its similarity to other reports ($j \neq k$). Similarly, for a given report x_t^k, $l^{x_t^k|x_v}$ aims to increase its similarity to its corresponding image and decrease its similarities to other images in the batch.

The local external loss, L_{ext}, aims to increase the similarity of positive pairs and decrease the similarity of negative ones, this time through the use of the local alignments. Thus, we use the aggregated local similarity score, $\mathcal{A}_{agg}$ (Section 3.3), instead of $\mathcal{A}_g$, as the objective for maximization and minimization, as illustrated in Figure 4.

The local internal loss, L_{int}, is given the local textual representation, t_j, as well as its corresponding attention weighted visual representation, u_j from Equation 3. It aims to improve the local representations by maximizing the similarity between corresponding pairs and minimizing the similarity between non-corresponding pairs of the same example. The loss is defined as follows:

$$L_{int}(x_v^k, x_t^k) = \sum_{j=1}^{N_w} (l_k^{t_j|u} + l_k^{u_j|t}),$$
$$l_k^{t_j|u} = -log\left(\frac{exp(a_j(t_j, u_j)/\tau)}{\sum_{i=1}^{N_w} exp(a_j(t_j, u_i)/\tau)} \right), \qquad (9)$$
$$l_k^{u_j|t} = -log\left(\frac{exp(a_j(t_j, u_j)/\tau)}{\sum_{i=1}^{N_w} exp(a_j(t_i, u_j)/\tau)} \right).$$

Here, for a local textual representation t_j, $l_k^{t_j|u}$ aims to increase the similarity between t_j and its corresponding visual weighted representation, u_j, and to decrease the similarity to other $u_{m \neq j}$ from the same study. The same rationale applies to $l_k^{u_j|t}$. We calculate $l_k^{t_j|u}$ and $l_k^{u_j|t}$ separately, for each image-report pair (x_v^k, x_t^k), as illustrated in Figure 5. Finally, we sum across all local pairs for a given study and then across all studies in the batch. Recall that the procedure described here is performed also for the visual representation in regards to the weighted textual representations.
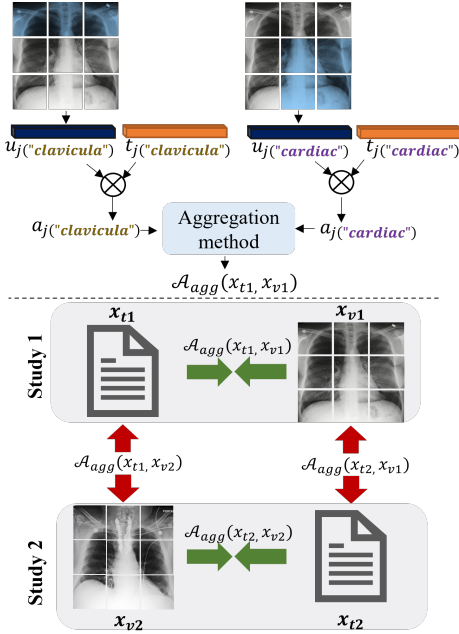
Figure 4: **Local external loss.** Top: Given a local textual representation t_j (clavicula) and its corresponding weighted visual representation u_j, we generate an aggregated alignment score $\mathcal{A}_{agg}$, based on the local alignments $\{a_j\}$. Bottom: $\mathcal{A}_{agg}$ is used to bring closer (green) the corresponding image-report pair (x_{t1}, x_{v1}) and farther away (red) non-corresponding pairs e.g., (x_{t1}, x_{v2}).
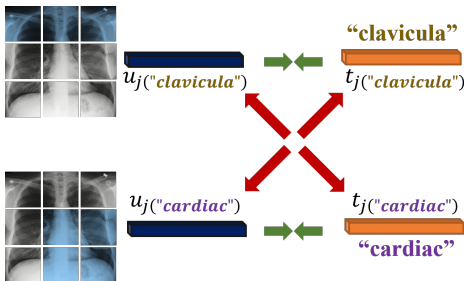

Figure 5: **Local internal loss.** Given local textual representations, t_j, and visual representations, u_j, this loss brings closer (green) corresponding representations, e.g. $t_{j("clavicula")}$ and $u_{j("clavicula")}$ and further apart (red) non-corresponding representations, e.g. $t_{j("cardiac")}$ and $u_{j("clavicula")}$, from the same example.

4. Experimental results

We examine our method on three retrieval applications: text-image retrieval, phrase-grounding, and class-based retrieval. For each application we compare against previous works that evaluate the specific application, as well as against additional methods that we trained. The supplementary material shows that our representations are also useful for classification.

Method	Image-to-Text			Text-to-Image		
	R@1	R@5	R@10	R@1	R@5	R@10
MGCA [23]	25.8	51.9	62.1	27.9	51.2	61.6
ConVIRT [27]	30.1	53.9	63.8	29.2	54.7	64.4
GLoRIA [8]	30.3	57.5	66.5	24.0	51.8	62.8
Ours w/o LT&PE	36.1	59.1	69.1	36.4	60.7	70.5
Ours	**39.7**	**63.2**	**71.7**	**37.7**	**62.1**	**71.3**

Table 1: **Text-Image retrieval results.** Given a report, our goal is to retrieve the matching image and vice versa. Our results outperform those of other methods on MIMIC-CXR, even without lateral (LT) images and structural information (PE). Our full method further improves the results.

Datasets. We ran our experiments on three datasets: *MIMIC-CXR*, *CheXpert 5X200*, and *MS-CXR*.

(1) *MIMIC Chest X-ray (MIMIC-CXR)* is a large, publicly available, dataset of chest radiographs, with free-text radiology reports [12]. The dataset contains $377,110$ images, corresponding to $227,835$ radiographic studies performed at the Beth Israel Deaconess Medical Center. Each study in the dataset contains a report and one or more images of *frontal* or *lateral*, where each study contains at least one frontal image. Each radiograph is associated with one or more classes, out of 14 optional diagnostic labels. The two main sections of interest of the report are *findings* and *impression*. Studies that do not contain these sections are filtered out. The data is randomly sampled to obtain validation and test sets, containing $1,000$ studies each. The remaining training set contains $205,000$ studies, of which $100,000$ have both frontal and lateral images.

(2) *CheXpert 5X200* contains 200 image-report pairs for 5 abnormality categories [8], sampled from the CheXpert dataset [10]. Each example in the dataset belongs to a single abnormality category.

(3) *MS-CXR* is a subset of MIMIC-CXR, which is extended for phrase-grounding [3]. It contains labeled (text descriptions) bounding boxes for each image. In total, there are $1,153$ pairs of region-text pairs.

Text-Image retrieval. Given a report, our goal is to find the most suitable image and vice versa. This task evaluates how close matching pairs are in the feature space. Hence, for this task, only the ground-truth image-report pairs are considered as positive. When both the frontal and the lateral images are available we use them both; when only one exists we fill the missing image with zeros. The accuracy of our model is measured by the $Recall@K$ metric, which returns the percentage of queries whose true match is successfully ranked within the top K matches.

Table 1 compares our performance on MIMIC-CXR to SoTA methods for representation learning, ConVIRT [27], GLORIA [8] and MGCA [23], which we have trained.

Method	Atelectasis	Cardio-megaly	Consoli-dation	Lung Opacity	Edema	Pneumo-nia	neumo-thorax	Pleural Effusion	Average
ConVIRT [27]	0.86	0.64	1.25	0.78	0.68	1.03	0.28	1.02	0.818
GLoRIA [8]	0.98	0.53	1.38	1.05	0.66	1.18	0.47	1.2	0.93
BioViL [3]	**1.17**	0.95	**1.45**	1.19	0.96	1.19	0.74	**1.5**	1.142
Ours	1.16	**1.18**	1.37	**1.37**	**1.05**	**1.27**	**1.01**	1.24	**1.206**

Table 2: **Phrase-grounding results.** Given a phrase and an image, the goal is to produce a similarity map between the phrase and the image. Our results outperform those of other methods, as reported in [3], on MS-CXR. The results are measured using CNR; higher values indicate good localization of the phrase in the image. Qualitative results can be found in the supplementary materials.

Our method outperforms other methods in R@1, R@5 and R@10, both for the image-to-text task and for the text-to-image task, even without utilizing structural knowledge and lateral images. Encoding domain structure and using the additional lateral images further improve the results.

Phrase-grounding. Given an image and a corresponding phrase, the goal is to produce an attention map of the similarity between the phrase and each image region [3]. The ground-truth is given as bounding boxes. Hence, this task evaluates the local alignments. Following [3], we measure the performance using *contrast to noise ratio (CNR)*, which measures the attention density inside the ground-truth bounding box. High values indicate that the network accurately detects the regions of interest for the given phrase. It is defined as:

$$CNR = |\mu_A - \mu_{\bar{A}}| / (\sigma_A^2 + \sigma_{\bar{A}}^2)^{\frac{1}{2}}, \qquad (10)$$

where A and $\bar{A}$ are the interior and exterior of the bounding box, and μ and σ are the mean and variance of the attention maps in each region.

Table 2 presents the results on the MS-CXR dataset. The results are presented for each of the 8 diagnostic categories, as well as for the average over the whole the dataset. Our performance is compared to that of BioViL [3], which introduced this task, and to the results of GLoRIA and ConVIRT that are reported in [3]. Note that BioViL uses a different text encoder (CXR-bert) from all other methods in the table (Bioclinical-Bert). Our model achieves SoTA results, demonstrating the strength of our local representations and the localization ability of our model.

Class-based retrieval. Given an image, our goal is to retrieve reports that belong to the same class of the image. For this task, a positive pair is defined as image-report that have the same abnormality label. We follow [8]'s settings, performing image-to-text retrieval and using the Precision@K metric to measure the accuracy of the retrieval. Precision@K is defined as the fraction of retrieved items (images) within the top K, which belong to the same class of abnormality as that of the query (textual descriptions).

Table 3 shows that our results outperform those of other

Method	Prec@5	Prec@10	Prec@100
ConVIRT [27]	30.8	28.2	22.2
GLoRIA [8]	32.6	33.4	**29.0**
MGCA [23]	29.3	27.6	22.4
Ours	**37.2**	**35.9**	28.8

Table 3: **Class-based retrieval results.** Given an image, reports that belong to the same class are retrieved. Our results outperform those of other methods on CheXpert 5X200 zero-shot evaluation. We note that this dataset contains only frontal views.

			Image-to-Text			Text-to-Image		
L_{int}	L_{ext}	L_g	R@1	R@5	R@10	R@1	R@5	R@10
		✓	31.8	58.2	66.8	33.6	58.0	68.0
✓		✓	33.3	57.3	67.8	33.2	58.5	67.3
✓	✓		33.2	58.4	68.0	31.5	57.9	67.9
✓	✓	✓	**36.1**	**59.1**	**69.1**	**36.4**	**60.7**	**70.5**

Table 4: **Loss ablation.** The best performance is achieved when combining all the three losses of Equation 1.

methods in almost all metrics. We note that [8] was originally trained and evaluated on the CheXpert dataset [10]. Since the reports of CheXpert are unavailable to the public, all models were trained on MIMIC-CXR [11] and evaluated in a zero-shot manner on the CheXpert 5X200 dataset.

5. Ablation study

This section evaluates the contribution of the different components of our method.

Losses. Our model optimizes a combination of three losses: global, local-internal and local-external (Equation 1). Table 4 demonstrates the contribution of each loss for both image-to-text and text-to-image retrieval tasks. The best performance is achieved by the combination of the three losses. Thus, attempting to achieve the three goals of these losses indeed improves the learning process.

Positional encoding. Recall that we utilize domain-specific

A diffuse reticular and nodular pattern has worsened and may reflect lymphangitic carcinomatosis in this patient with history of malignancy. Cardiomediastinal contours are stable. Moderate right pleural effusion has increased in size with adjacent right basilar atelectasis and or consolidation. A small left pleural effusion is apparently new.

The patient has known cystic fibrosis. The perihilar area of bronchiectasis with peribronchial thickening are stable. Pre-existing peribronchial opacities in the right upper lobe have minimally increased. Signs of overinflation, better appreciated on the lateral radiograph, continue to be present. No pleural effusions. Normal size of the cardiac silhouette.
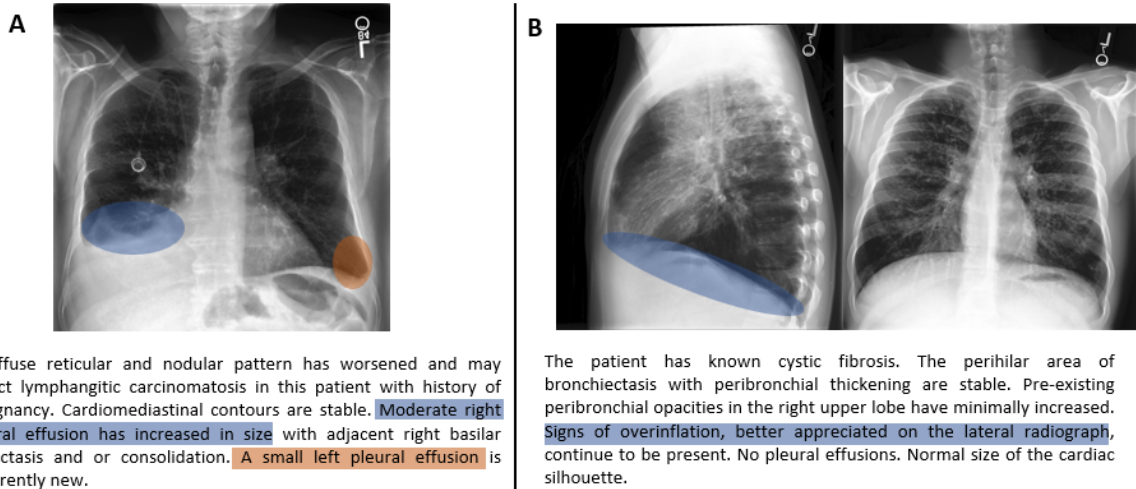
Figure 6: **Domain-knowledge importance.** (A) The positional information enables the model to consider the signs of right pleural effusion (blue) and small left pleural effusion (orange). Thanks to our positional encoding, our model succeeds in the text-image retrieval task, but would fail otherwise. (B) The visual clue, the flattened diaphragm, which is a sign of over-inflation appears only in the lateral image (highlighted in blue). Thanks to the lateral view, our model succeeds in the text-image retrieval task; it would fail if it used only the frontal image.

		Image-to-Text			Text-to-Image		
LT	PE	R@1	R@5	R@10	R@1	R@5	R@10
		36.1	59.1	69.1	36.4	60.7	70.5
	✓	37.7	61.5	70.7	34.7	60.9	70.5
✓		38.1	61.6	**72.1**	37.3	61.2	**71.5**
✓	✓	**39.7**	**63.2**	71.7	**37.7**	**62.1**	71.3

Table 5: **Domain knowledge.** Adding either lateral (LT) images or visual structure information (PE) to the baseline frontal images improves the results in both tasks.

knowledge by adding positional encoding vectors. Table 5 shows that positional encoding improves the results in most metrics. It is beneficial both when using a single view or two views. Figure 6(A) demonstrates the contribution of positional encoding qualitatively. When the report contains relevant location information "moderate right pleural effusion" (blue) and "small left pleural effusion" (orange), without positional encoding, our base model might fail to align the report and the image. However, when trained with positional encoding, the alignment is successful.

Lateral images. Lateral images are explicitly mentioned in many reports, hence using them (when available) is desirable. Table 5 confirms this, by showing superior results across all metrics, compared to using only the frontal images. Figure 6(B) shows an example in which when our model is trained without lateral images, the alignment between the report and the image fails. Using both views results in a correct alignment. The report mentions signs of overinflation that are "better appreciated on the lateral ra-

diograph" (blue). The signs for overinflation in the lateral image are more evident than in the frontal image.

Limitations. Similarly to [3, 18], the limitation of our approach is that it does not explicitly deal with false negatives in the contrastive losses. That is to say, there may be multiple reports that match a given image (and vice versa), but only one is considered positive.

6. Conclusions

This paper presented a new model for learning a joint X-ray image & report representation. The model is based on a new alignment scheme that considers both local and global information. In addition, we propose to enrich the model with domain-specific information.

The benefits of our representation is demonstrated on three types of retrieval tasks, two of which require large precision: text-image retrieval, phrase-grounding, and class-based retrieval. Our model is shown to outperform SoTA models, even when the additional knowledge is unavailable. The domain-specific knowledge adds to performance.

In the future, we would like to study loss functions that allow an image (/text) to be paired to multiple mates from the other domain. For instance, the contrastive loss should not push away normal images from normal text of different pairs. This has the potential to improve results across tasks and datasets, especially those of low diversity.

References

[1] Society for imaging informatics in medicine: Siim-acr pneumothorax segmentation.

[2] Emily Alsentzer, John R. Murphy, Willie Boag, Wei-Hung Weng, Di Jin, Tristan Naumann, and Matthew B. A. McDermott. Publicly available clinical BERT embeddings. *CoRR*, abs/1904.03323, 2019.

[3] Benedikt Boecking, Naoto Usuyama, Shruthi Bannur, Daniel C. Castro, Anton Schwaighofer, Stephanie Hyland, Maria Wetscherek, Tristan Naumann, Aditya Nori, Javier Alvarez-Valle, Hoifung Poon, and Ozan Oktay. Making the most of text semantics to improve biomedical vision–language processing. In *Lecture Notes in Computer Science*, pages 1–21. Springer Nature Switzerland, 2022.

[4] Haiwen Diao, Ying Zhang, Lin Ma, and Huchuan Lu. Similarity reasoning and filtration for image-text matching. *CoRR*, abs/2101.01368, 2021.

[5] Alexey Dosovitskiy, Lucas Beyer, Alexander Kolesnikov, Dirk Weissenborn, Xiaohua Zhai, Thomas Unterthiner, Mostafa Dehghani, Matthias Minderer, Georg Heigold, Sylvain Gelly, Jakob Uszkoreit, and Neil Houlsby. An image is worth 16x16 words: Transformers for image recognition at scale. *CoRR*, abs/2010.11929, 2020.

[6] Yifan Du, Zikang Liu, Junyi Li, and Wayne Xin Zhao. A survey of vision-language pre-trained models. *arXiv preprint arXiv:2202.10936*, 2022.

[7] Kaiming He, Xiangyu Zhang, Shaoqing Ren, and Jian Sun. Deep residual learning for image recognition. *CoRR*, abs/1512.03385, 2015.

[8] Shih-Cheng Huang, Liyue Shen, Matthew P Lungren, and Serena Yeung. GLoRIA: A Multimodal Global-Local Representation Learning Framework for Label-efficient Medical Image Recognition.

[9] Yan Huang, Qi Wu, and Liang Wang. Learning semantic concepts and order for image and sentence matching. *CoRR*, abs/1712.02036, 2017.

[10] Jeremy Irvin, Pranav Rajpurkar, Michael Ko, Yifan Yu, Silviana Ciurea-Ilcus, Chris Chute, Henrik Marklund, Behzad Haghgoo, Robyn L. Ball, Katie S. Shpanskaya, Jayne Seekins, David A. Mong, Safwan S. Halabi, Jesse K. Sandberg, Ricky Jones, David B. Larson, Curtis P. Langlotz, Bhavik N. Patel, Matthew P. Lungren, and Andrew Y. Ng. Chexpert: A large chest radiograph dataset with uncertainty labels and expert comparison. *CoRR*, abs/1901.07031, 2019.

[11] Alistair EW Johnson, Tom J Pollard, Lu Shen, Li-wei H Lehman, Mengling Feng, Mohammad Ghassemi, Benjamin Moody, Peter Szolovits, Leo Anthony Celi, and Roger G Mark. Mimic-iii, a freely accessible critical care database. *Scientific data*, 3(1):1–9, 2016.

[12] Alistair E. W. Johnson, Tom J. Pollard, Seth J. Berkowitz, Nathaniel R. Greenbaum, Matthew P. Lungren, Chih-ying Deng, Roger G. Mark, and Steven Horng. MIMIC-CXR, a de-identified publicly available database of chest radiographs with free-text reports. *Scientific Data*, 6(1):317, dec 2019.

[13] Andrej Karpathy and Li Fei-Fei. Deep visual-semantic alignments for generating image descriptions. *CoRR*, abs/1412.2306, 2014.

[14] Kuang-Huei Lee, Xi Chen, Gang Hua, Houdong Hu, and Xiaodong He. Stacked cross attention for image-text matching. *CoRR*, abs/1803.08024, 2018.

[15] Kunpeng Li, Yulun Zhang, Kai Li, Yuanyuan Li, and Yun Fu. Visual semantic reasoning for image-text matching. *CoRR*, abs/1909.02701, 2019.

[16] Xiujun Li, Xi Yin, Chunyuan Li, Pengchuan Zhang, Xiaowei Hu, Lei Zhang, Lijuan Wang, Houdong Hu, Li Dong, Furu Wei, Yejin Choi, and Jianfeng Gao. Oscar: Object-semantics aligned pre-training for vision-language tasks. *CoRR*, abs/2004.06165, 2020.

[17] Jong Hak Moon, Hyungyung Lee, Woncheol Shin, Young-Hak Kim, and Edward Choi. Multi-modal Understanding and Generation for Medical Images and Text via Vision-Language Pre-Training.

[18] Philip Müller, Georgios Kaissis, Congyu Zou, and Daniel Rueckert. Joint learning of localized representations from medical images and reports. *CoRR*, abs/2112.02889, 2021.

[19] George Shih, Carol wu, Safwan Halabi, Marc Kohli, Luciano Prevedello, Tessa Cook, Arjun Sharma, Judith Amorosa, Veronica Arteaga, Maya Galperin-Aizenberg, Ritu Gill, Myrna Godoy, Stephen Hobbs, Jean Jeudy, Archana Laroia, Palmi Shah, Dharshan Vummidi, Kavitha Yaddanapudi, and Anouk Stein. Augmenting the national institutes of health chest radiograph dataset with expert annotations of possible pneumonia. *Radiology: Artificial Intelligence*, 1:e180041, 01 2019.

[20] Rebecca Smith-Bindman, Diana L. Miglioretti, and Eric B. Larson. Rising Use Of Diagnostic Medical Imaging In A Large Integrated Health System. *Health Affairs*, 27(6):1491–1502, nov 2008.

[21] Aäron van den Oord, Yazhe Li, and Oriol Vinyals. Representation learning with contrastive predictive coding. *CoRR*, abs/1807.03748, 2018.

[22] Ashish Vaswani, Noam Shazeer, Niki Parmar, Jakob Uszkoreit, Llion Jones, Aidan N Gomez, Łukasz Kaiser, and Illia Polosukhin. Attention is all you need. *Advances in neural information processing systems*, 30, 2017.

[23] Fuying Wang, Yuyin Zhou, Shujun Wang, Varut Vardhanabhuti, and Lequan Yu. Multi-granularity cross-modal alignment for generalized medical visual representation learning. *arXiv preprint arXiv:2210.06044*, 2022.

[24] Linda Wang, Zhong Qiu Lin, and Alexander Wong. Covidnet: A tailored deep convolutional neural network design for detection of covid-19 cases from chest x-ray images. *Scientific reports*, 10(1):1–12, 2020.

[25] Zifeng Wang, Zhenbang Wu, Dinesh Agarwal, and Jimeng Sun. Medclip: Contrastive learning from unpaired medical images and text. *arXiv preprint arXiv:2210.10163*, 2022.

[26] Zhiyun Xue, Sema Candemir, Sameer Antani, L. Long, Stefan Jaeger, Dina Demner-Fushman, and George Thoma. Foreign object detection in chest x-rays. pages 956–961, 11 2015.

[27] Yuhao Zhang, Hang Jiang, Yasuhide Miura, Christopher D. Manning, and Curtis P. Langlotz. Contrastive Learning of Medical Visual Representations from Paired Images and Text. oct 2020.